Electronic Supplementary Information (ESI)

Multifunctional quaternized carbon dots with enhanced biofilm penetration and eradication efficiencies

Huan-Huan Ran,† Xiaotong Cheng,† Yan-Wen Bao, Xian-Wu Hua, Ge Gao, Xiaodong Zhang, Yao-Wen Jiang, Ya-Xuan Zhu and Fu-Gen Wu*

State Key Laboratory of Bioelectronics, School of Biological Science and Medical Engineering, Southeast University, 2 Sipailou Road, Nanjing 210096, P. R. China E-mail: wufg@seu.edu.cn

†Huan-Huan Ran and Xiaotong Cheng contributed equally to this work.

Additional figures

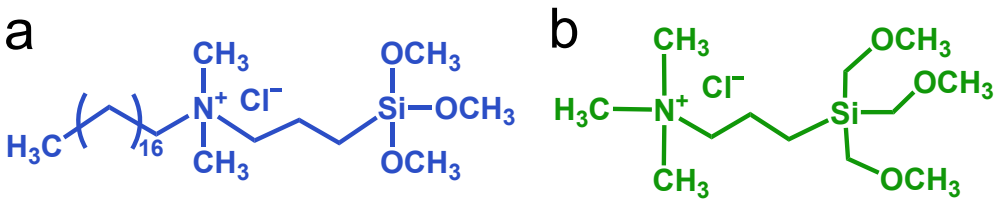

Fig. S1 Molecular structures of Si-QAC (a) and TTPAC (b).

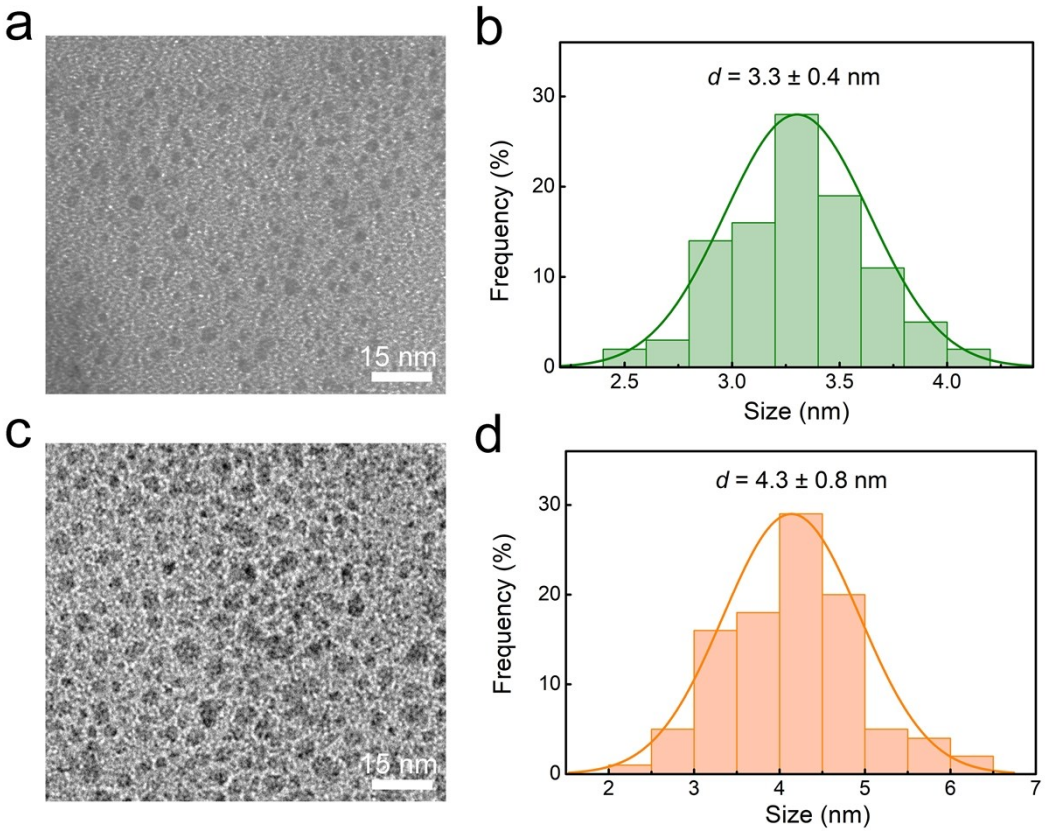

Fig. S2 (a) TEM image and (b) corresponding size distribution histogram of Si-QAC CDs. (c) TEM image and (d) corresponding size distribution histogram of TTPAC CDs.

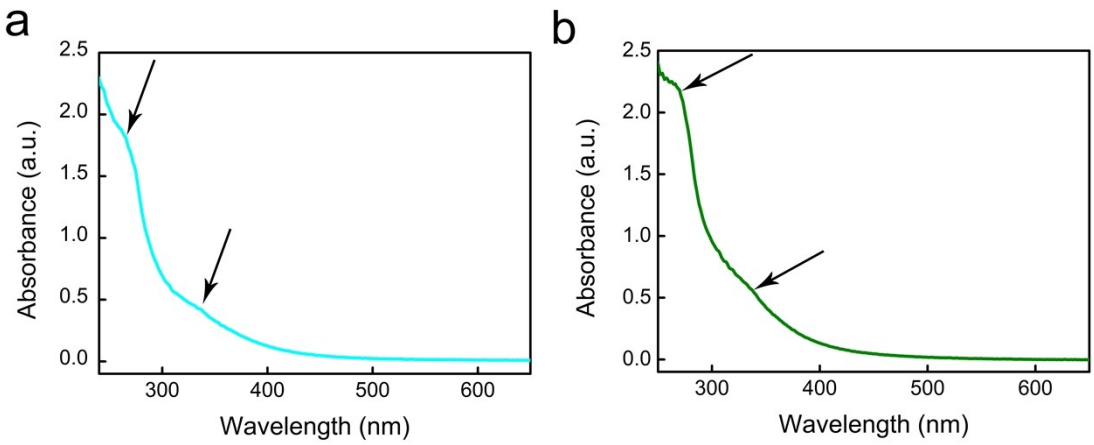

Fig. S3 UV−vis absorption spectra of Si-QAC CDs (a) and TTPAC CDs (b) in water.

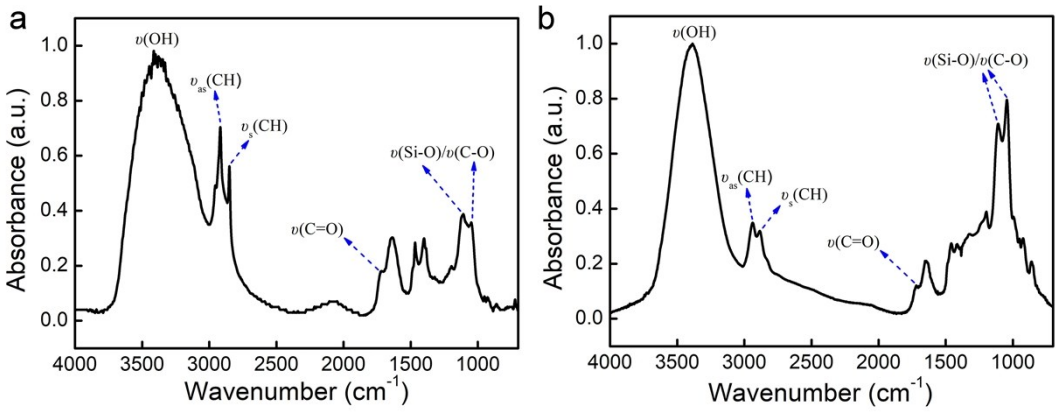

Fig. S4 FTIR spectra of Si-QAC CD (a) and TTPAC CD (b) dry powders.

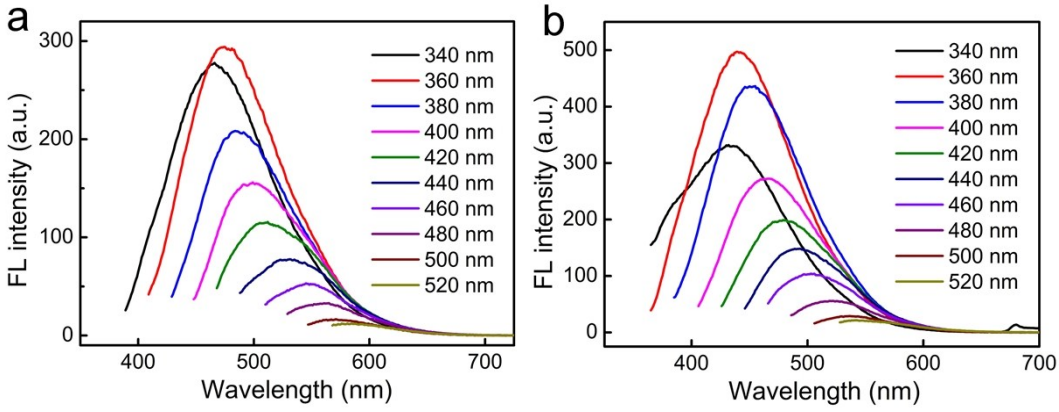

Fig. S5 Fluorescence (FL) emission spectra of Si-QAC CDs (a) and TTPAC CDs (b) in water at different excitation wavelengths (340–520 nm).

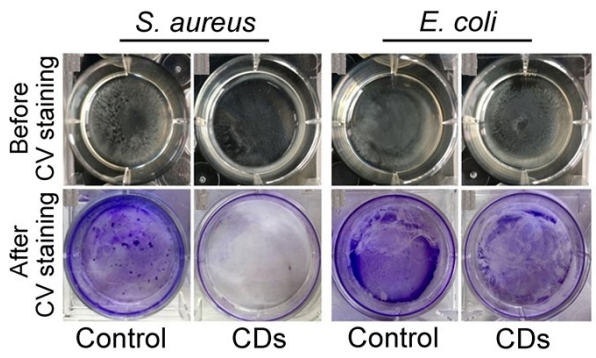

Fig. S6 Photographs of the untreated (control) and Si-QAC CD (1000 μg mL^{-1})-treated *S. aureus* and *E. coli* biofilms for 24 h before and after crystal violet (CV) staining.

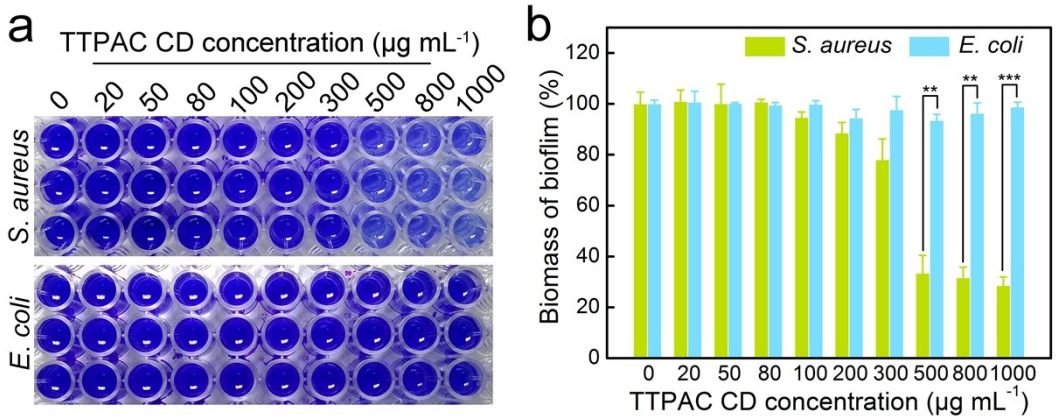

Fig. S7 (a) Photographs of the CV staining assay results of *S. aureus* and *E. coli* bacterial biofilms after treatment with different concentrations of TTPAC CDs for 24 h. (b) Change of biofilm biomass as a function of TTPAC CD concentration. The biofilm biomass was quantified by the CV absorbance of the bacterial biofilms in (a). The biomass of the untreated biofilm was set to be 100%. $^{**}p < 0.01$, $^{***}p < 0.001$.

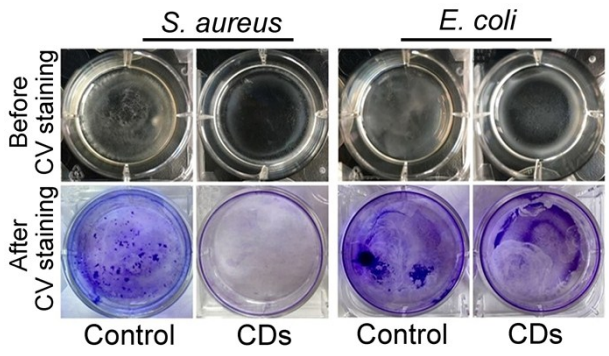

Fig. S8 Photographs of the untreated (control) and Si-QAC CD (1000 μg mL^{-1})-treated *S. aureus* and *E. coli* bacteria for 72 h before and after CV staining.

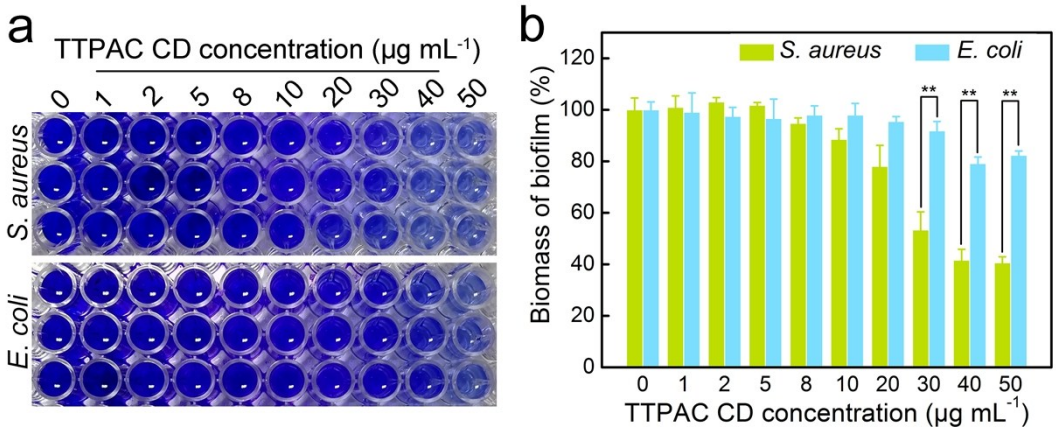

Fig. S9 (a) Photographs of the CV staining assay results of *S. aureus* and *E. coli* bacteria after treatment with different concentrations of TTPAC CDs for 72 h. (b) Change of biofilm biomass as a function of TTPAC CD concentration. The biofilm biomass was quantified by the CV absorbance of the bacterial biofilms in (a). The biomass of the untreated biofilm was set to be 100%. $^{**}p < 0.01$.

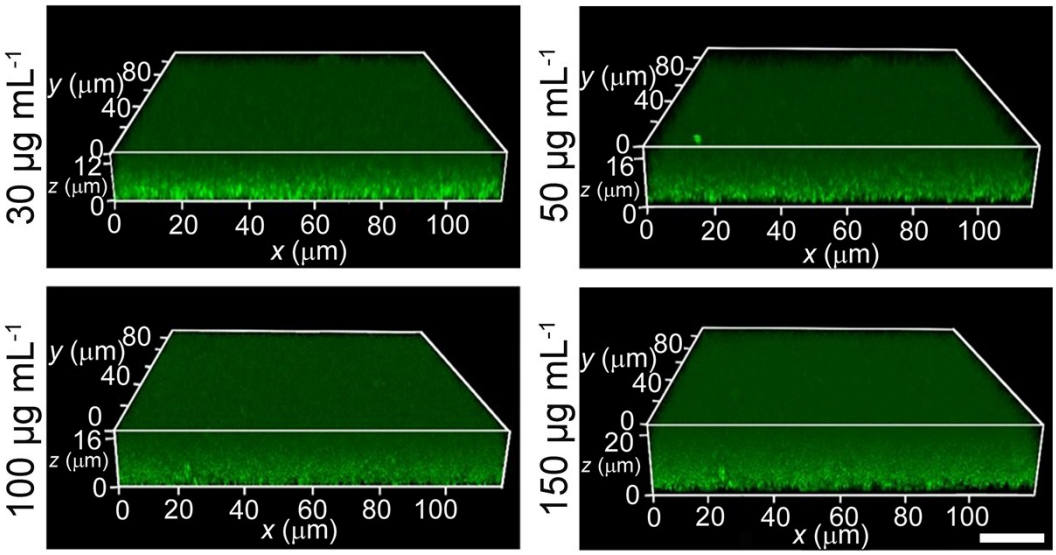

Fig. S10 3D confocal fluorescence images of *S. aureus* biofilms taken after being stained with different concentrations of Si-QAC CDs for 2 h under an excitation wavelength of 488 nm to determine the appropriate CD concentration for biofilm imaging. Scale bar: 20 μm.

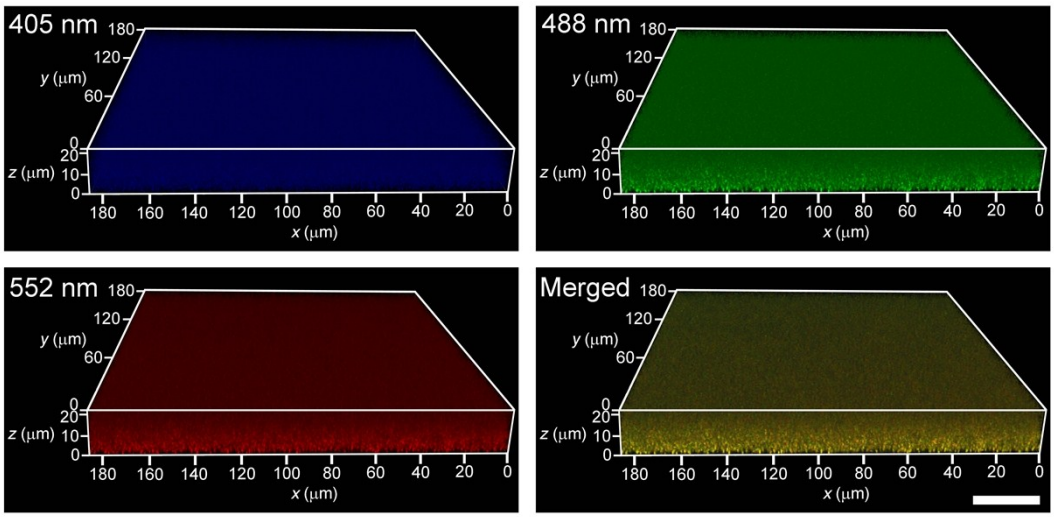

Fig. S11 3D confocal fluorescence images of an *E. coli* biofilm treated with Si-QAC CDs (50 μg mL^{-1}) for 2 h at different excitation wavelengths (405, 488 and 552 nm). Scale bar: 30 μm.

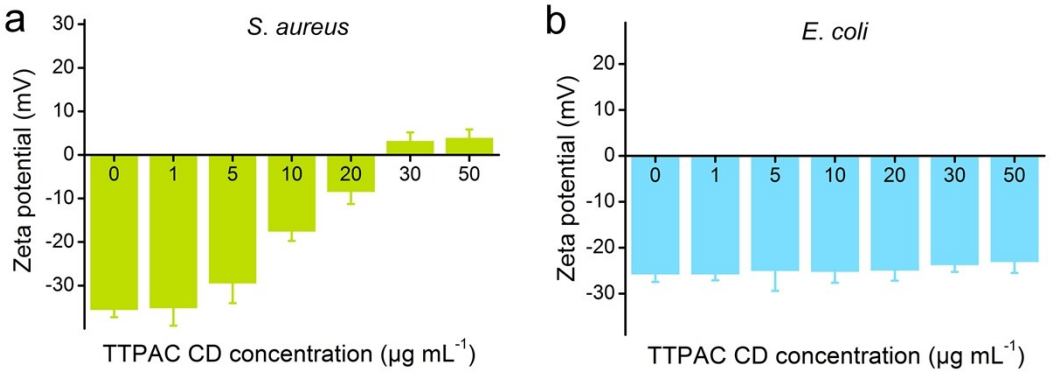

Fig. S12 Zeta potentials of *S. aureus* (a) and *E. coli* (b) bacteria after incubation with different concentrations of TTPAC CDs (0−50 μg mL^{-1}) for 2 h.

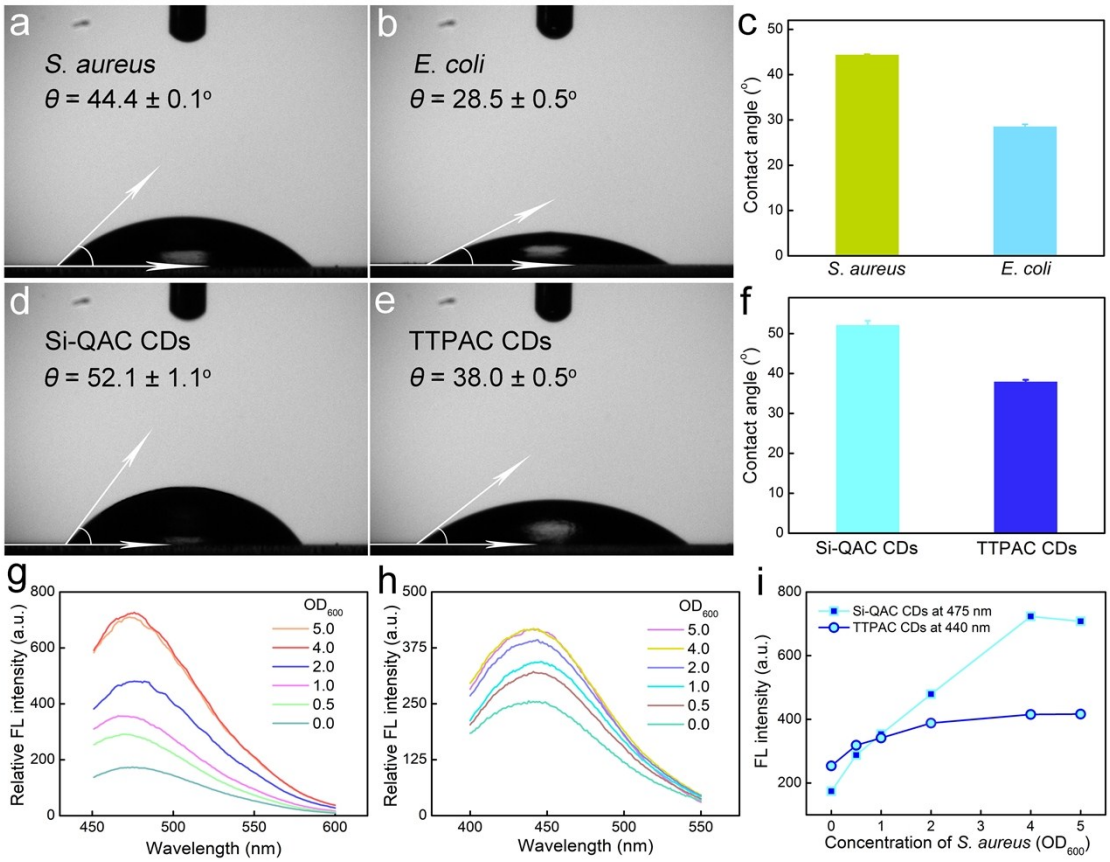

Fig. S13 Photographs of a water droplet on a glass slide coated with an *S. aureus* bacterial layer (a) and a water droplet on a glass slide coated with an *E. coli* bacterial layer (b), and corresponding statistical histogram of the contact angles (c). Photographs of a water droplet on a glass slide coated with an Si-QAC CD layer (d) and a water droplet on a glass slide coated with a TTPAC CD layer (e), and corresponding statistical histogram of the contact angles (f). (g) FL spectra of Si-QAC CDs (6 μg mL^{-1}) in the presence of different concentrations (OD_{600} = 0.0–5.0) of *S. aureus* bacteria. (h) FL spectra of TTPAC CDs (6 μg mL^{-1}) in the presence of different concentrations (OD_{600} = 0.0–5.0) of *S. aureus* bacteria. (i) Corresponding statistical results of the FL intensities in (g) at 475 nm and in (h) at 440 nm, respectively.

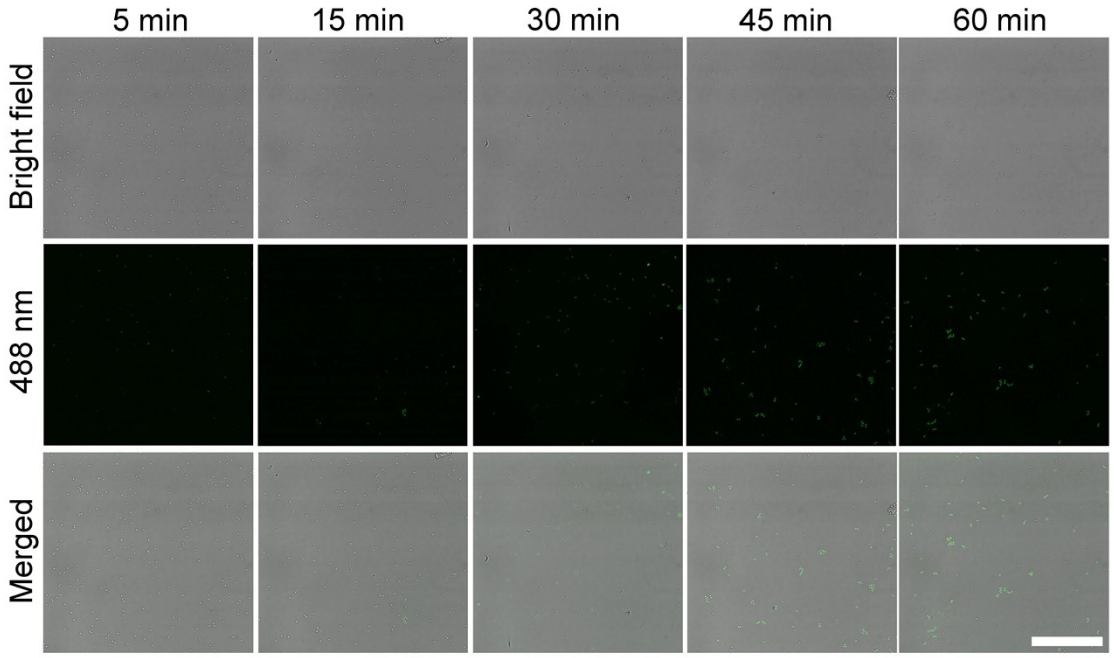

Fig. S14 Confocal images of *S. aureus* bacteria after incubation with TTPAC CDs (20 μg mL^{-1}) for different time periods. Scale bar: 40 μm.